Black carbon radiative heating effects on cloud microphysics and implications for aerosol indirect forcing: 1. Extended Köhler theory

William C. Conant, Athanasios Nenes and John H. Seinfeld

Departments of Chemical Engineering and Environmental Science and Engineering, Mail Code 210-41, California Institute of Technology, Pasadena, California, 91125, USA

Abstract. Black carbon (BC) aerosol absorbs sunlight that might have otherwise been reflected to space and changes the radiative heating of the atmosphere and surface. These effects may alter the dynamical and hydrological processes governing cloud formation. A new, *microphysical*, effect of BC on climate is identified here, in which solar heating within BC-containing cloud condensation nuclei (CCN) slows or prevents the activation of these CCN into cloud drops. Solar-heated BC-containing droplets are elevated in temperature by fractions of a degree above the ambient, thus raising the droplet vapor pressure, and inhibiting activation of the most absorptive CCN. This paper develops the theory describing the alteration of the Köhler curve (i.e. the equilibrium vapor pressure over a droplet as a function of water uptake) as a function of CCN size and chemical composition (BC fraction, in particular). The effect is most significant in those CCN that contain volumes of BC larger than a 500 nm diameter sphere. For an aerosol population with 10% BC mass fraction per particle, solar heating can cause a 10% reduction in the CCN concentration at 0.01% critical supersaturation. On the other hand, the effect of heating by BC absorption on CCN activation above about 0.1% critical supersaturation is negligible.

1. Introduction

Atmospheric aerosols reduce the solar radiation absorbed by the Earth through direct and indirect mechanisms (Figures 1a-d). In the direct effect, aerosols scatter radiation to space that would have otherwise heated the surface or atmosphere (Fig. 1a). In the indirect effect, increased concentrations of cloud condensation nuclei (CCN) alter the microphysical properties of clouds, enhancing cloud reflectivity (Fig. 1b). Additional indirect effects on clouds have been proposed that involve aerosol-induced changes in precipitation, radiative heating, and atmospheric dynamics (Figs. 1c-d). In contrast, absorptive particles, black carbon (e.g. soot) in particular, exert a positive (warming) climate forcing (Figs. 1e-g). Uncertainties in the distribution of natural and anthropogenic aerosols, their chemical speciation, and the aerosol-cloud-climate interactions they induce presently constitute the largest source of uncertainty in climate models that attempt to predict the role of anthropogenic emissions on climate.

Carbonaceous particles are an important class of primary aerosol emitted into the atmosphere. These particles tend to be a complex mixture of graphitic material and organic compounds. The graphitic component, called soot or black carbon, is characterized by significant absorption of solar radiation. Freshly emitted black carbon particles tend to be hydrophobic; as they age in the atmosphere they tend to acquire a hydrophilic coating. As black carbon becomes sufficiently hydrophilic, it is able to form cloud droplets upon activation in a supersaturated environment. Black carbon can play a role in indirect aerosol radiative forcing in two ways: (1) BC particles absorb solar radiation, changing the vertical and horizontal thermal structure of the atmosphere and surface, changes that can have an impact on dynamical processes governing cloud formation and evaporation; (2) Those particles that act

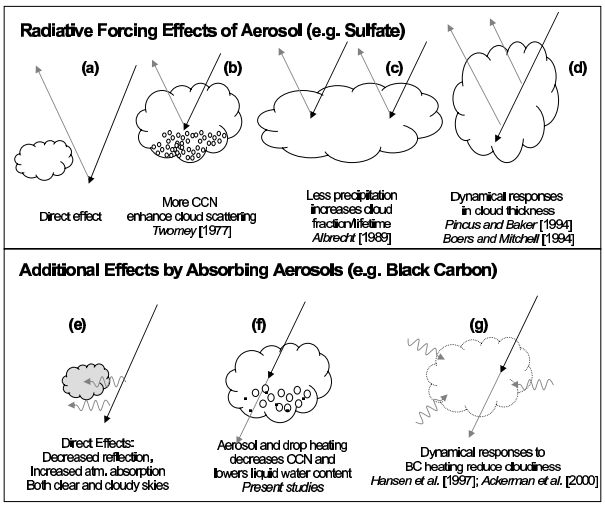

Figure 1. Direct and indirect radiative effects of aerosol, divided into those effects unrelated to aerosol absorption **(a)-(d)**, and those related to aerosol absorption **(e)-(g)**.

as CCN and become incorporated in cloud droplets absorb solar radiation and heat the droplets and the air around them, processes that can potentially alter cloud activation itself. Effect (1) was identified in the INDOEX campaign through observation and modeling of absorptive species [*Ackerman et al.*, 2000; *Lelieveld et al.*, 2001]. Effect (2) is the subject of this and a companion paper [*Nenes et al.*, 2002].

2. Theoretical development

Köhler theory [*Köhler*, 1921; *Seinfeld and Pandis*, 1998] predicts the equilibrium water vapor pressure of an aqueous droplet containing solute given its physical and chemical properties, and hence can be used to predict the exchange of water vapor between the droplet and the ambient atmosphere during cloud formation. The Köhler equations are most often implemented under the assumption that radiative heating of the droplet is negligible [*Fuchs*, 1959]. Absorption and emission of solar and infrared radiation by liquid water have since been found to play an important role in the evolution of the drop size distribution near cloud top [*Harrington et al.* [2000], and references therein]. However, these studies treat the droplet absorption spectrum as that of pure water and do not address the presence of black carbon in the seed aerosol.

This study examines how radiative heating by black carbon within a particle affects equilibrium Köhler theory. Effects of non-BC absorption (e.g. H_2O and H_2SO_4 absorption in the near infrared) and longwave radiative effects are neglected to isolate the perturbation by BC. The effect of this perturbation on the time-dependent (non-equilibrium) cloud activation problem is treated in a companion paper [*Nenes et al.*, 2002] using a cloud parcel model with explicit microphysics that includes the effect of BC heating on parcel thermodynamics.

2.1. Heating by Black Carbon

Black carbon (BC) is the most efficient aerosol species at absorbing solar radiation. Aged anthropogenic aerosol often contains 5% to 20% black carbon by mass [*O'Dowd et al.*, 1993; *Novakov et al.*, 2000; *Hitzenberger and Tohno*, 2001]. Aged atmospheric BC particles are rarely pure, externally mixed, species, but are most often found to be coated with water soluble compounds such as sulfate and organic carbon [*Posfai et al.*, 1999]. BC is produced by incomplete combustion in the form of 10 nm – 50 nm diameter spherules that agglomerate into chains [*Medalia et al.*, 1983]. In well-aged aerosol, the bulk of the BC mass is contained in particle sizes from 300 to 700 nm diameter through coagulation, coalescence in evaporated cloud drops, and addition of secondary aerosol mass [*Kaneyasu and Murayama*, 2000]. Because this size range encompasses that of particles most likely to serve as CCN, we investigate the impact of droplet solar heating on the properties of BC-containing CCN.

To compute the droplet heating for BC-containing aerosols, we represent the internally mixed BC aerosol as a layered sphere with a black carbon core of diameter D_c coated by a hydrophilic sulfate shell of diameter D_p (Figure 2). The heating rate for each particle, Φ (W), is obtained from

$$\Phi = \int_{0.2\mu m}^{5\mu m} I(\lambda)\sigma_a(\lambda)d\lambda \qquad (1)$$

where $I(\lambda)$ is the spectral actinic flux (spherically integrated spectral intensity) having units W m^{-2} nm^{-1}, and $\sigma_a(\lambda)$ is the particle absorption cross-section (m^2), and solar wavelength, λ, is assumed to range from 0.2 to 5 μm. For the purposes of this study, $I(\lambda)$ is predicted by a 38-band multi-spectral Monte Carlo radiative transfer model [*Podgorny et al.*, 2000], which assumes a sub-tropical marine atmosphere over ocean, an aerosol optical depth of 0.3 (at 0.5 μm), and no clouds; the model described by *Podgorny et al.* [2000] has been slightly modified here to predict actinic flux instead of irradiance. To test the sensitivity of actinic flux to these

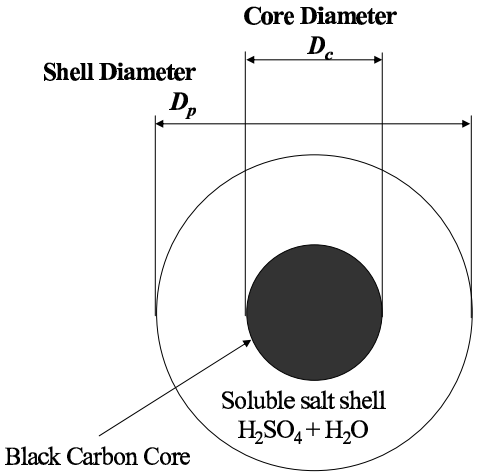

Figure 2. Concentric shell geometry assumed for the calculation of droplet heating.

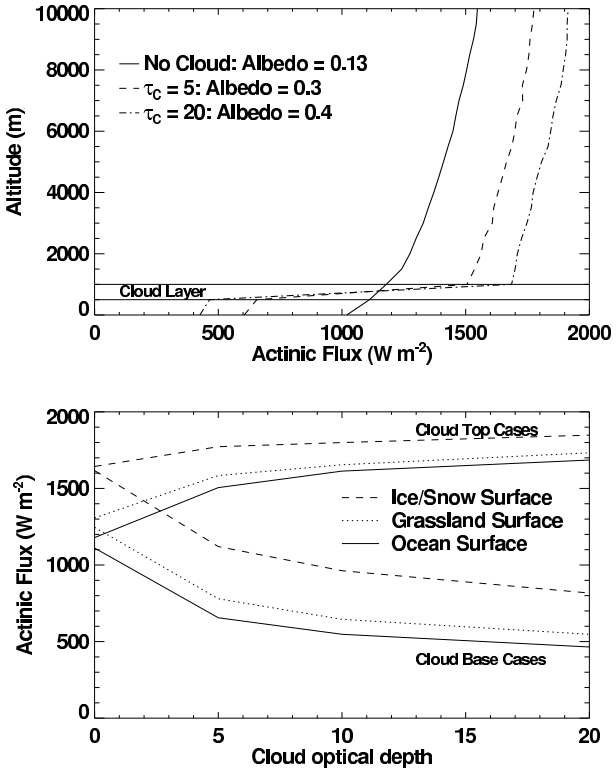

Figure 3. Actinic flux under varying conditions of cloudiness and surface albedo. **(a)** Vertical profile of actinic flux calculated for 3 cases: no cloud, cloud with optical thickness (τ_c) = 5, and cloud with τ_c = 20. Each case considers a solar zenith angle of 60 ° , ocean surface reflection (albedo ∼0.07 for no cloud case), and clouds are horizontally homogeneous. **(b)** Actinic flux for cloud base and cloud top as a function of cloud optical depths ranging from 0 (no cloud) to 20. Three cases of surface albedo are considered: ocean reflection (explicitly accounting for both Fresnel and bulk reflection), (b) grassland (isotropic albedo of 0.26), and (c) snow/ice (isotropic albedo of 0.6).

assumptions, Figures 3a,b illustrate the variation of actinic flux with surface type and the presence of clouds. Fig. 3a illustrates that actinic flux varies by about a factor of two from cloud base to cloud top, with peak fluxes occurring at cloud top. Fig. 3a considers only ocean, whereas Fig 3b shows that cloud base and cloud top actinic flux are also sensitive to surface albedo. Together, Figs. 3a and 3b show that the actinic flux of 1000 W m^{-2} assumed in the remainder of this paper (except where stated otherwise) is appropriate for clear-sky cases and thin clouds, will be a slight overestimate for the base of moderately well established clouds over ocean or land, and will be a slight underestimate for cases at or above cloud top or over bright surfaces.

The particle absorption cross-section, $\sigma_a(\lambda)$, is computed for each particle as a function of D_p and D_c using a 2-layer radiative parameter model based on Mie theory [*Toon and Ackerman*, 1981]. *Fuller et al.* [1999] show that the concentric geometry assumed here overestimates absorption by at most 15% compared to a randomly placed encapsulated inclusion, and that the treatment of the carbon as a single sphere instead of an agglomeration of spherules underestimates the absorption by at most 30%. BC located near the edge of the droplet could enhance the heating an order of magnitude beyond that considered here [*Chýlek et al.*, 1996]. Indices of refraction for BC, sulfate, and water are obtained from *Hess et al.* [1998]. The imaginary index of refraction for BC used here (0.45 at 0.55 μm) is on the

lower end of observed values [*Fuller et al.*, 1999; *Marley et al.*, 2001]. Shell index of refraction is a function of aerosol hydration, and is determined based on the molar ratios and indices of refraction for sulfate and water, following *Tang* [1997].

2.2. Droplet Equilibrium Temperature

The equilibrium temperature of a (static) aerosol particle of diameter D_p is governed by the balance between net radiative heat absorbed by the particle, Φ, and the sensible heat flux conducted away from the particle, $F(\mathrm{W\ m^{-2}})$,

$$\Phi = \pi D_p^2 F. \tag{2}$$

Through scaling arguments it can be shown that the temperature profiles both within the droplet and in the surrounding gas phase, for typical atmospheric conditions, are in steady state. As a result, F depends on ΔT, the difference between the particle surface temperature, T_p, and the ambient temperature, T_a, far from the particle as follows,

$$F = 2k_{air}^{'}\frac{\Delta T}{D_p}, \tag{3}$$

where $k_{air}^{'}$ is the thermal conductivity of air corrected for the non-continuum effect. (The non-continuum effect reduces thermal conductivity for sub-micron or high-altitude particles.)

Combining (2) and (3) yields the dependence of equilibrium particle surface temperature perturbation on radiative heating,

$$\Delta T = \frac{\Phi}{2\pi D_p k_{air}^{'}}. \tag{4}$$

2.3. Modification to the Köhler Equation

The temperature perturbation by radiative heating raises the vapor pressure over the surface of the particle; the resulting modification to Köhler theory has been discussed elsewhere [*Ackerman et al.*, 1995; *Harrington et al.*, 2000]. The Köhler equation expresses the equilibrium vapor pressure over an aerosol surface, $p_w(T_p, D_p)$, in reference to $p^\circ(T_p)$, the vapor pressure over a flat surface of pure water at the same temperature T_p [*Seinfeld and Pandis*, 1998],

$$\ln\left(\frac{p_w\left(T_p, D_p\right)}{p^\circ(T_p)}\right) = \frac{4M_w\sigma}{RT_p\rho_w D_p} - \frac{6n_s M_w}{\pi\rho_w\left(D_p^3 - D_c^3\right)} \tag{5}$$

where M_w is the molecular weight of water, σ is the surface tension of the droplet, ρ_w is the density of water, R is the ideal gas constant, and n_s is the number of moles of solute in the shell. D_c is the geometric diameter of any insoluble core, and D_p varies due to condensation and evaporation of water. The first term on the right side of (5) describes the tendency for the vapor pressure to increase over a curved surface (Kelvin effect), and the second term expresses the vapor pressure depression caused by the solute mole fraction (Raoult effect).

Particle saturation, S_p, is defined as the ratio of particle surface vapor pressure to vapor pressure of water over a surface at ambient temperature, $p^\circ(T_a)$,

$$\ln S_p = \ln\left(\frac{p_w\left(T_p, D_p\right)}{p^\circ(T_a)}\right). \tag{6}$$

Without radiative heating, $T_a = T_p$, (5) and (6) are equivalent, and (5) can be used to obtain the particle saturation. In the presence of heating, the relationship between $p^\circ(T_a)$ and $p^\circ(T_p)$ must be accounted for using the Clausius-Clapeyron relation [*Seinfeld and Pandis*, 1998],

$$\ln\left(\frac{p^\circ(T_p)}{p^\circ(T_a)}\right) = \frac{\Delta H M_w}{RT_a^2}\Delta T, \tag{7}$$

where ΔH is the latent heat of condensation and $\Delta T \ll T_a$. Combining (4)-(7) yields the modified Köhler equation in the presence of radiative heating,

$$\ln S_p = \frac{\frac{4M_w\sigma}{RT_p\rho_w D_p} - \frac{6n_s M_w}{\pi\rho_w\left(D_p^3 - D_c^3\right)} + \frac{\Delta H M_w}{RT_a^2}\frac{\Phi}{2\pi k_{air}^{'} D_p}}{}. \tag{8}$$

The last term in (8) is the solar heating term. Equation (7) provides the dominant source of sensitivity of equilibrium particle saturation to elevated droplet temperature. For comparison, Table 1 lists the magnitude of other, minor effects that arise from either variations in droplet properties with temperature or from simplifications made deriving equilibrium saturation (8). These minor effects will be neglected in the remainder of this study.

Because of its inverse dependence on D_p, we can express the heating effect as a modification to the Kelvin effect term in the Köhler equation,

$$\ln S_p = \frac{4M_w\sigma}{RT\rho_w D_p}\left(1 + \gamma_a\right) - \frac{6n_s M_w}{\pi\rho_w\left(D_p^3 - D_c^3\right)}, \tag{9}$$

where we define the aerosol *heating parameter*, γ_a, as,

Table 1.

Temperature Sensitive parameter	$\frac{d \ln S_p}{d\Delta T}$	Sensitivity (K^{-1})
Clausius-Clapeyron effect	$\frac{\Delta H M_w}{R T_a^2}$	6.2×10^{-2}
Gas-phase temperature gradient effects	$<$ order $\left(\frac{1}{T_a}\right)$	$< 3.4\times10^{-3}$
Water density	$-\left(\frac{A}{D_p} - \frac{B}{D_p^3 - d_p^3}\right)\frac{d \ln \rho_w}{dT_a}$	2.4×10^{-4} lnS_p $< 10^{-6}$ for ln$S_p < .4\%$
Temperature sensitivity of Kelvin effect	$-\frac{A}{D_p T_a}$	$-$ 7.5×10^{-7}
Water-air surface tension	$\frac{A}{D_p}\frac{d \ln \sigma_w}{dT_a}$	$-$ 4×10^{-7}

$$\gamma_a \equiv \frac{\Delta H \rho_w \Phi}{8\pi k_{air}' T_a \sigma}. \tag{10}$$

In the limit that $\Phi \rightarrow 0$, $\gamma_a \rightarrow 0$ and (9) reduces to the traditional Köhler equation (5).

It is convenient at this point to consider the absorption efficiency, Q_{abs}, defined as the ratio of the absorption cross-section to the physical cross-section,

$$Q_{abs} = \frac{4}{\pi}\frac{\sigma_a}{D_p^2}, \tag{11}$$

which generally can range from 0 to order unity, tending asymptotically to 1 for large, perfectly absorptive particles. In Figure 4, the heating parameter is shown as a function of dry particle diameter, d_p, and absorption efficiency. For the purpose of calculating the Kelvin effect, the surface tension of the droplet is assumed to be that of water. Also shown in Figure 4 is the absorption efficiency calculated for aerosols of mixed BC and sulfate (H_2SO_4) composition; two cases are shown, one with 50% BC by mass, the with 10% BC by mass. The purpose of these calculations is to illustrate reasonable heating parameters expected for a given dry particle diameter, and hence define the conditions in which the effect is most likely to be important. When γ_a =1, the heating effect is equal in magnitude to the Kelvin effect. For the conditions described above, γ_a =1 for a 3.5 μm (dry) particle that is 10% BC by mass. The heating parameter presented in Figure 4, which is computed for dry aerosol, will generally be lower than that for an activated particle due to the enhancement of BC heating when included within a droplet. This amplification is predicted by the model described in Section 2.1. and will be included when calculating droplet heating.

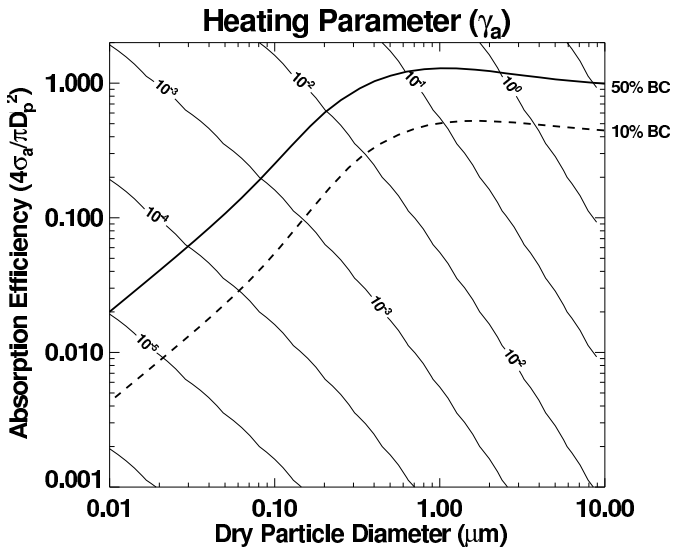

Figure 4. Heating parameter, γ_a, for dry particles (contour lines) as a function of dry particle diameter, d_p, and spectrally averaged absorption efficiency, Q_{abs}. The heavy solid and dashed lines represent the relationship between Q_{abs} and d_p for dry aerosols composed of 50% BC by mass and 10% BC, respectively.

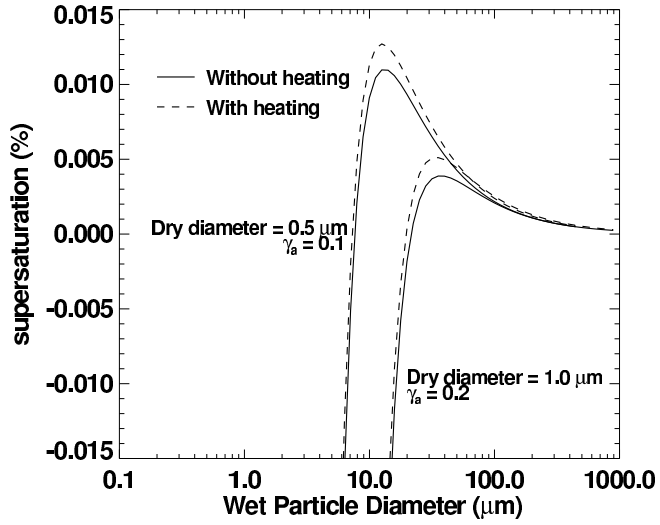

Figure 5. Effect of droplet heating on the Köhler curves of particles of 0.5 μm and 1.0 μm dry diameter. Heating parameters of 0.1 and 0.2 are chosen for the two droplet sizes, respectively. The solid curve represents the no-heating case, the dashed curve represents the heating case. Particles are assumed to have the hygroscopic properties of sulfate.

2.4. Effect of black carbon radiative heating on critical supersaturation

Figure 5 illustrates the effect of droplet heating on the Köhler curves for dry particle diameters of 0.5 μm and 1.0 μm and γ_a values of 0.1 and 0.2. These curves correspond to particles with the hygroscopic properties of pure sulfate. Droplet heating has the effect of increasing the maximum equilibrium saturation of the droplet (i.e. critical saturation, S_c), above which the droplet is unstable to condensational growth. Thus the effect of the heating is to delay activation of the aerosol into a cloud drop. Note, however, that for these large droplet sizes, the unactivated aerosol is already comparable in size to cloud drops, and should be treated as such for radiative purposes [*Nenes et al.*, 2001].

A value for γ_a above which heating can become important can be quantified in terms of the change in particle critical saturation in the presence of heating. If the critical diameter is much larger than the diameter of the insoluble core, then the particle critical saturation ratio without the heating source, S_c^{wo}, can be computed by classical Köhler theory,

$$\ln S_c^{wo} = \left(\frac{4A^3}{27B}\right)^{1/2} \tag{12}$$

where $A = 4M_w\sigma/RT\rho_w$, and $B = 6n_sM_w/\pi\rho_w$. Similarly, in the presence of the internal heat source, the critical saturation ratio, S_c^w, is given by (12) with A multiplied by the factor $(1+\gamma_a)$,

$$\frac{\ln S_c^w}{\ln S_c^{wo}} = (1+\gamma_a)^{3/2} \tag{13}$$

By expanding $\ln S = \ln(1+s) \approx s$, where s is the supersaturation, the ratio of particle critical supersaturation with and without heating is given by,

$$\frac{s_c^w}{s_c^{wo}} = (1+\gamma_a)^{3/2} \tag{14}$$

In a similar fashion, it can be shown that the ratio of critical diameter with heating, D_{pc}^w, to that without heating, D_{pc}^{wo}, is given by,

$$\frac{D_{pc}^w}{D_{pc}^{wo}} = (1+\gamma_a)^{-1/2} \tag{15}$$

Figures 6a and 6b show the critical supersaturation and critical diameter as functions of dry particle diameter, d_p, for two cases: (1) 10% BC and 90% sulfate; and (2) 50% BC, 50% sulfate. For each case, the results are shown both with and without the effect of heating (i.e. daytime and nighttime cases, respectively). The first effect of the BC inclusion is to reduce the mass of solute, hence increasing critical supersaturation with increasing BC fraction irrespective of the heating. This is identified in Figure 6a as the "solute effect", seen as the difference in supersaturation between the two cases where heating is not introduced. The difference between the daytime and nighttime cases, identified as the "heating effect", is greatest for the largest particles for which heating parameter is greatest (Fig. 4). The heating effect is further isolated by considering particles of fixed composition under conditions of varying solar irradiance. Figures 7a and 7b illustrate the sensitivity of critical supersaturation to actinic fluxes varying from 0 W m^{-2} (nighttime) to 1500 W m^{-2}, for the 50% BC and 10% BC cases, respectively. For these cases actinic flux is scaled uniformly across the solar spectrum.

One interesting result seen in Figs. 6a and 7 is the local minimum in the dependence of s_c on d_p. This minimum, s_{low}, occurs for particles of dry diameter d_{low}. This is a result of the assumption of fixed BC mass fraction in the dry particle. In unheated particles, the

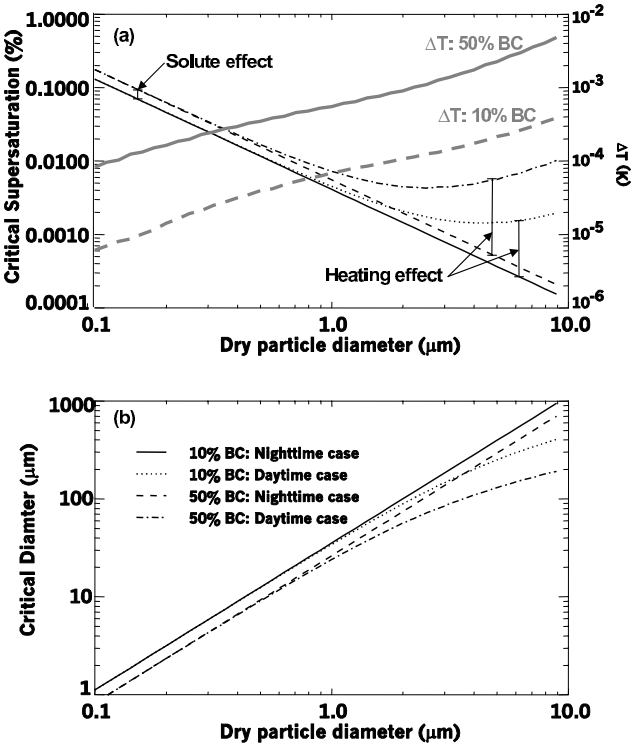

Figure 6. Effect of BC on **(a)** Critical supersaturation, and **(b)** Critical diameter. Four cases are considered: (1) 10% BC by mass and no heating; (2) 10% BC and heating by a 1000 Wm-2 actinic flux; (3) and (4) same as (1) and (2) but for 50% BC by mass. The difference between the no heating cases (1) and (3) is caused by the reduced sulfate mass in the 50% BC case compared to the 10% BC case. The heating effect is apparent as a divergence between the heating and no heating cases towards large particle sizes. The perturbation in droplet temperature at critical diameter is shown as the thick, gray lines in (a). The legend in (b) applies to both (a) and (b).

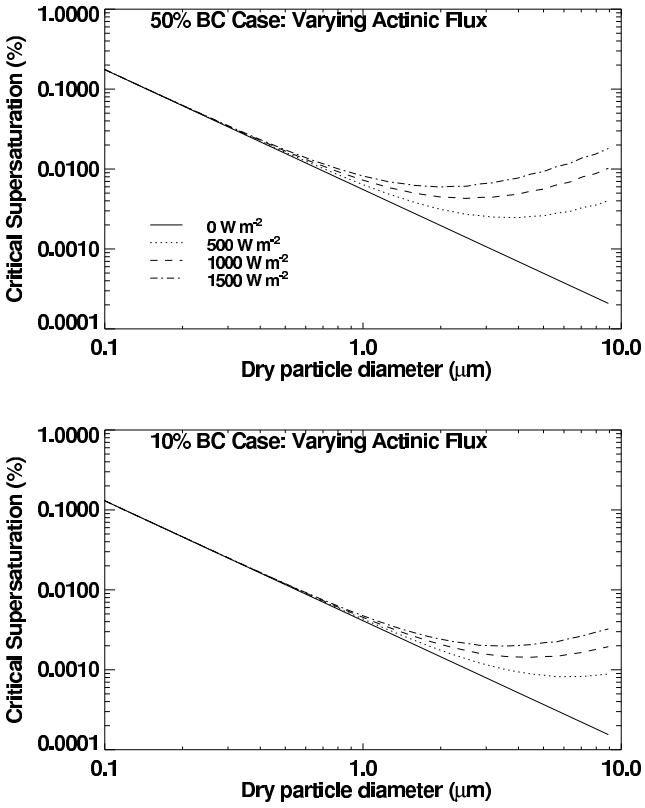

Figure 7. Illustration of the impact of actinic flux on critical supersaturation for **(a)** 50% BC by mass, and **(b)** 10% BC by mass. The effect of increasing actinic flux is to increase the lowest possible critical supersaturation, s_{low}, for particles of a given composition and to decrease the dry particle diameter, d_{low}, at which this minimum occurs.

critical supersaturation monotonically decreases with increasing d_p. However, BC heating increases approximately with d_p^2 for supermicron particles, and eventually dominates over the Raoult term, leading to an increase in s_c with d_p for the largest sizes. We can obtain some insight by including the heating effect into (12) and differentiating with respect to dry particle diameter,

$$\frac{\partial \ln s_c}{\partial d_p} = \frac{\partial}{\partial d_p}\left[\frac{3}{2}\ln A + \frac{3}{2}\ln\left(1+\gamma_a\right) - \frac{1}{2}\ln B\right]. \quad (16)$$

Note that A, the Kelvin effect term, is insensitive to dry particle diameter if we ignore surface active species; B, the Raoult term, increases with d_p^3 due to increased moles of solute; and, γ_a increases with d_p^2, for the supermicron particles considered here. It can be shown from (16) and the above assumptions that d_{low} occurs where $\gamma_a = 1$, and thus (16) yields two regimes for the dependence of s_c on d_p based on γ_a.

$$\begin{array}{lll} \frac{\partial \ln s_c}{\partial d_p} = -\frac{1}{2}d_p; & \gamma_a \ll 1 and & d_p \ll d_{low} \\ \frac{\partial \ln s_c}{\partial d_p} = \frac{3}{2}d_p; & \gamma_a \gg 1 \quad and & d_p \gg d_{low} \end{array} . \quad (17)$$

For $\gamma_a \ll 1$, the change in supersaturation with dry diameter is dominated by the Raoult term, and s_c decreases with increasing d_p, as expected from the classical solution. However, for $\gamma_a \gg 1$, the heating term dominates over the Raoult term, and s_c increases with dry diameter. For the case of 10% BC mass fraction, $d_{low} \cong 4\mu$m, meaning dry particles at 4 μm have the lowest s_c relative to larger and smaller particles. For clouds with slow cooling rates, this suppression of the activation of the largest CCN may impact the rate at which the larger particles uptake liquid water, with potentially important effects on the water mass balance during cloud formation.

The magnitude of the change in critical supersaturation is shown in Figure 8 as a function of the dry particle diameter and absorption efficiency. The relationship between dry diameter and absorption efficiency for the two cases of 50% BC and 10% BC are repeated in Figure 8. The magnitude of critical supersaturation increase for 10% BC aerosol ranges from 10^{-4}% to about 2×10^{-3}% as aerosol dry diameter ranges from 0.3 μm to 10 μm. The maximum impact of heating shown here is to elevate the critical supersaturation of 10 μm 50% BC particles by 0.01 percentage units, which can be compared to the 0.02%-0.25% median critical supersaturation associated with marine cumulus cloud drops [*Twohy and Hudson*, 1995].

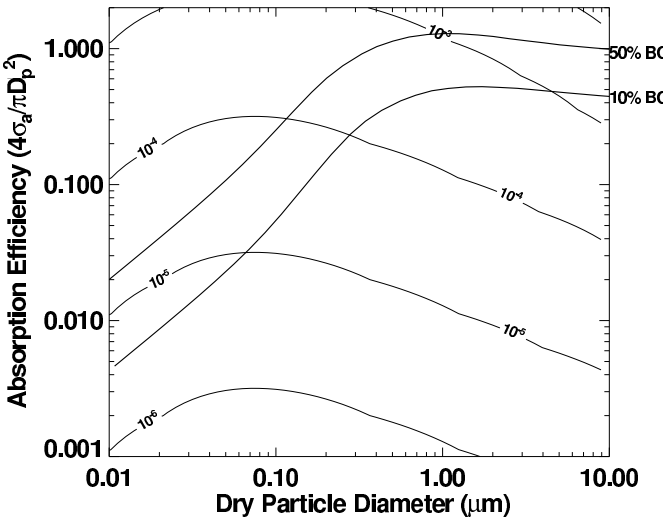

Figure 8. Change in critical supersaturation computed for dry particles as a function of particle diameter and absorption efficiency, Q_{abs}. Contours delineate values of Δs_c. The solid and dashed lines represent the relationship between Q_{abs} and d_p for dry aerosols composed of 100% BC and 10% BC, respectively. The calculation of Δs_c includes the enhancement of heating caused by the encapsulation of the soot core in the droplet.

3. Effect of black carbon radiative heating on CCN spectra

To understand the implications of droplet heating for cloud activation, we consider the change in the CCN supersaturation spectrum for three aerosol distributions. The CCN supersaturation spectrum $N_{CCN}(s_c)$ is that property of an aerosol population defined as the number of particles (cm^{-3}) that have critical supersaturations less than s_c. $N_{CCN}(s_c)$ is a monotonically increasing function of s_c, and approaches the total aerosol concentration as $s_c \to \infty$. The three cases considered here are based on modeled and observed size distributions and varying assumptions about BC heating. The first two cases comprise three-mode log-normal size distributions from the observations of *Whitby* [1978] that were chosen to represent urban and clean continental aerosols.

The third case uses size distributions of North Indian Ocean aerosol observed from ship during the Indian Ocean Experiment (INDOEX) [*Ramanathan et al.*, 2001]. Extensive observations of aerosol size distribution, composition, and mixing state were made, affording a detailed analysis of the BC heating effect in this region where BC ranged from 10%-15% of the dry aerosol

mass [*Novakov et al.*, 2000; *Lelieveld et al.*, 2001]. Size distribution measurements are taken from the tandem differential mobility analyzer and aerodynamic particle size measurements of *Bates et al.* [2001]. Each aerosol particle is assumed to be an internal mixture of BC and sulfate, based on findings using time-of-flight aerosol mass spectrometry that each BC particle was coated with sulfate and/or organics, and few anthropogenic particles were found without soot inclusions [*Lelieveld et al.*, 2001]. (This treatment neglects the presence of pure seasalt aerosol, which may have been more prevalent than anthropogenic particles at the largest sizes.)

Figure 9a-c illustrates the supersaturation spectrum, $N_{CCN}(s_c)$, calculated for pure sulfate, 10% BC, and 50% BC for each of the size distributions described above. Some of the differences seen between the three compositional cases can be explained by the solute effect that was illustrated in Fig. 6, and some of the differences are due to the heating effect. For each case that includes the radiative heating, $N_{CCN}(s_c)$ remains 0 until s_c exceeds the threshold critical supersaturation s_{low}. The effect of BC radiative heating on the supersaturation spectrum is isolated from solubility effects in Figs. 9(d)-(f) by illustrating the percent change in supersaturation spectrum from the nighttime case (no heating) to the daytime case (actinic flux of $\sim$1000 W m^{-2}). Despite the variations in the aerosol size distributions considered here, we consistently see that the 10% BC case predicts a 1% reduction in CCN for $s_c = 0.03\%$ supersaturation, and that the 50% BC case predicts a 7%-10% reduction in CCN at this supersaturation. For all cases, the change in supersaturation spectrum is less than 1% for values of s_c exceeding 0.08%.

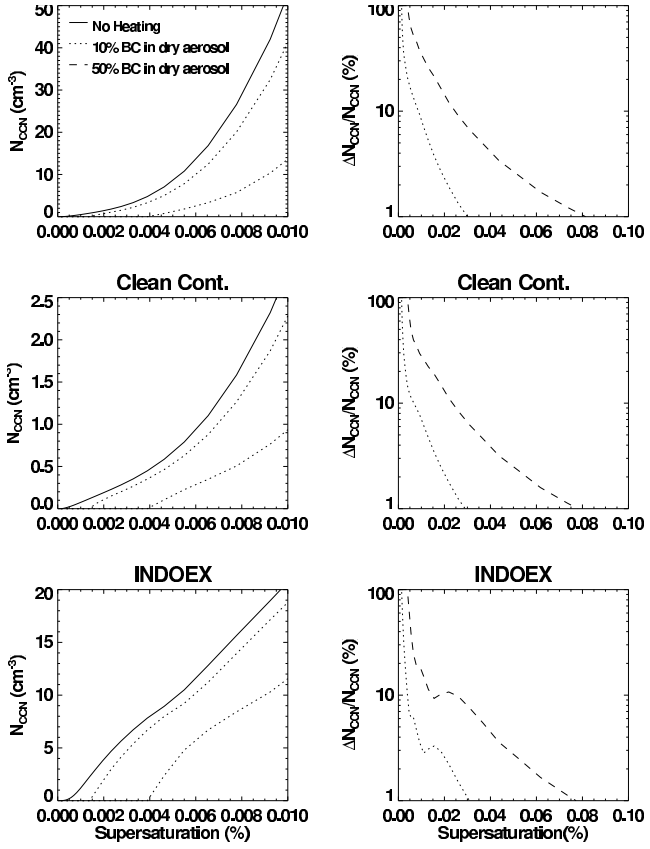

Figure 9. (a)-(c) CCN spectrum calculated from size distributions assuming each particle is either pure sulfate, 10% BC by dry mass, or 50% BC. Cases (a)-(b) are calculated from *Whitby* [1978] size distributions, case (c) from INDOEX. Effects of BC seen in (a)-(c) are partially due to the solute effect (see Fig. 6.) **(d)-(f)** BC heating effect on CCN spectrum. The percent perturbation in CCN spectrum between nighttime (no heating) and daytime (heating) corresponding to (a)-(c), respectively, are shown as a function of supersaturation for both the 10% BC and 50% BC cases.

4. Effect of radiative heating on time-dependent droplet activation

This study has addressed the equilibrium Köhler theory that is the foundation for theory and models of cloud and droplet activation. The following discussion demonstrates the applicability of the equilibrium theory described above to the non-equilibrium equations underpinning cloud activation theory.

Droplet activation theory is expressed by the equations relating energy and mass flux between the droplet and the ambient atmosphere. The time-rate of change of temperature is given by the energy balance,

$$m_p c_w \frac{dT_p}{dt} = \Phi - 2\pi k_{air}^{'} D_p \left(T_p - T_a\right) + \Delta H \frac{dm_p}{dt}. \quad (18)$$

The term on the left is the rate of change of internal particle energy, where m_p is the particle mass and c_w is the heat capacity of water (J kg^{-1} K^{-1}). The terms on the right side of (18) are, respectively, the radiative heating from equation (1), the conductive heat loss from equations (2) and (3), and the condensational heat gain, where changes in mass are assumed to be solely due to condensation/evaporation. Note that in steady-state, m_p and T_p are constant in time, and equation (18) reduces to (4). Scaling arguments can be used to show that the heat content term plays a minor role in the energy balance. Thus the temperature difference $\Delta T = T_p - T_a$, can be obtained in terms of the equilibrium temperature difference from (4), (hereafter ΔT_{eq}) plus the effect of condensational heating, ΔT_{con},

$$\Delta T = \frac{\Phi + \Delta H \frac{dm_p}{dt}}{2\pi D_p k'_{air}} = \Delta T_{eq} + \Delta T_{con} \qquad (19)$$

The time rate of change of particle mass is governed by diffusion of water vapor to/from the droplet surface, which is conventionally expressed as proportional to the difference in water vapor concentration between the droplet and the ambient [*Seinfeld and Pandis*, 1998]. Thus, the mass flux in the presence of a small temperature gradient is,

$$\begin{aligned} &\tfrac{dm_p}{dt} = \rho_w \tfrac{\pi}{2} D_p^2 \tfrac{dD_p}{dt} = \\ &= 2\pi D_p \tfrac{D'_v}{RT_a} \left[p_{w,a} - \tfrac{T_a}{T_p} p_w(T_p, D_p) \right] \end{aligned} \qquad (20)$$

where $p_{w,a}$ is the ambient vapor pressure, and D'_v is the diffusivity of water vapor in air corrected for non-continuum effects and the mass accommodation coefficient. For the steady-state case, (20) prescribes zero net vapor concentration gradient. The equations for the equilibrium Köhler curve in the presence of radiative heating, (6)-(8), when combined with (20) yield,

$$\begin{aligned} &D_p \tfrac{dD_p}{dt} = \\ &= \tfrac{4 M_w D'_v}{\rho_w} \tfrac{p^\circ(T_a)}{RT_a} \left[S_a - S_p \tfrac{T_a \exp\left(\frac{\Delta H M_w}{RT_a^2} \Delta T_{con} \right)}{T_a + \Delta T_{con}} \right] \end{aligned} \qquad (21)$$

where S_a is the ambient saturation and S_p is the particle equilibrium saturation. The term to the right of S_p is due to modification of particle saturation due to condensational heating. Because ΔT_{con} is proportional to droplet growth rate (19) and $\Delta T_{con} \ll T_a$, we have (after some algebra),

$$D_p \frac{dD_p}{dt} = \frac{S_a - S_p}{\frac{\rho_w R T_a}{4 p^\circ(T_a) D'_v M_w} + \frac{\Delta H \rho_w}{4 k'_a T_a} \left(\frac{\Delta H M_w}{R T_a} - 1 \right)} \qquad (22)$$

Equation (22) is identical to the growth equation in the absence of radiative heating [*Seinfeld and Pandis*, 1998]. The radiative effect is contained within the modified equilibrium particle saturation, S_p, defined in (8), subject to the simplifications quantified in Table 1. Thus, the effects of radiative heating on droplet growth rate can be implemented using the modified Köhler curve, obviating the need to explicitly calculate the time-dependent droplet temperature perturbation.

5. Conclusion

In this study we have examined the effect of the radiative heating of black carbon (BC) on the critical supersaturation spectrum of internally mixed aerosol. Radiative heating raises the critical supersaturation of BC-containing CCN, thus reducing the number of particles available for activation at a given maximum supersaturation. The effect is found to be strongest for large aerosol particles with high BC mass fractions. For a 10% BC dry mass fraction at all aerosol sizes, over several aerosol size distributions considered, only about a 1% reduction in CCN is predicted at 0.03% critical supersaturation. At a critical supersaturation of 0.01%, the reduction in CCN can be nearly 10%. This equilibrium heating effect is expected to be most important for clouds formed at low cooling rates (e.g. stratus clouds and radiative fogs). Although we did not consider the case of contrails or high altitude stratiform clouds here, we can speculate that the heating effect may be important in their formation due to high observed BC fractions [*Posfai et al.*, 1999], low thermal diffusivity, and high actinic fluxes. Perturbations to the supersaturation spectrum are known to have highly nonlinear effects on the resulting cloud drop concentration, and hence indirect radiative forcing [*O'Dowd et al.*, 1999]. To assess the impact of black carbon radiative heating on cloud albedo, *Nenes et al.* [2002] incorporate radiative heating into a detailed cloud parcel model that explicitly accounts for the complex processes linking cloud albedo to the aerosol on which the cloud forms.

Acknowledgments. This work was supported by Office of Naval Research grant N00014-96-1-0119.

References

Ackerman, A., O. Toon, and P. Hobbs, A model for particle microphysics, turbulent mixing, and radiative transfer in the stratocumulus-topped marine boundary layer and comparisons with measurements, *J. Atmos. Sci.*, *52*, 1204–1236, 1995.

Ackerman, A., O. Toon, D. Stevens, A. Heymsfield, V. Ramanathan, and E. Welton, Reduction of tropical cloudiness by soot, *Science*, *288*, 1042–1047, 2000.

Bates, T., P. Quinn, D. Coffman, J. Johnson, T. Miller, D. Covert, A. Wiedensohler, S. Leinert, A. Nowak, and C. Neususs, Regional physical and chemical properties of the marine boundary layer aerosol across the atlantic during Aerosols99: An overview, *J. Geophys. Res.*, *106*, 20,767–20,782, 2001.

Chýlek, P., G. Lesins, G. Videen, J. Wong, R. Pinnick, D. Ngo, and J. Klett, Black carbon and absorption of solar radiation by clouds, *J. Geophys. Res.*, *101*, 23,365–23,371, 1996.

Fuchs, N., *Evaporation and Droplet Growth in Gaseous Media*, Pergamon Press, New York, 1959.

Fuller, K., W. Malm, and S. Kreidenweis, Effects of mixing on extinction by carbonaceous particles, *J. Geophys. Res.*, *104*, 15,941–15,954, 1999.

Harrington, J., G. Feingold, and W. Cotton, Radiative impacts on the growth of a population of drops within simulated summertime arctic stratus, *J. Atmos. Sci.*, *57*, 766–785, 2000.

Hess, M., P. Koepke, and I. Schult, Optical properties of aerosols and clouds: The software package OPAC, *Bull. Am. Met. Soc*, *79*, 831–844, 1998.

Hitzenberger, R., and S. Tohno, Comparison of black carbon (BC) aerosols in two urban areas - concentrations and size distributions, *Atmos. Environ.*, *35*, 2153–, 2001.

Kaneyasu, N., and S. Murayama, High concentrations of black carbon over middle latitudes in the North Pacific Ocean, *J. Geophys. Res.*, *105*, 19,881–19,890, 2000.

Köhler, H., Zur kondensation des wasserdampfe in der atmosphäre, *Geofys. Publ.*, *2*, 3–15, 1921.

Lelieveld, J., P. Crutzen, V. Ramanathan, M. Andreae, C. Brenninkmeijer, T. Campos, G. Cass, R. Dickerson, H. Fischer, J. de Gouw, A. Hansel, A. Jefferson, D. Kley, A. de Laat, S. Lal, M. Lawrence, J. Lobert, O. Mayol-Bracero, A. Mitra, T. Novakov, S. Oltmans, K. Prather, T. Reiner, H. Rodhe, H. Scheeren, D. Sikka, and J. Williams, The indian ocean experiment: Widespread air pollution from south and southeast asia, *Science*, *291*, 1031–1036, 2001.

Marley, N., J. Gaffney, C. Baird, C. Blazer, P. Drayton, and J. Frederick, An empirical method for the determination of the complex refractive index of size-fractionated atmospheric aerosols for radiative transfer calculations, *Aerosol Sci Technol.*, *34*, 535–549, 2001.

Medalia, A., D. Rivin, and D. Sanders, A comparison of carbon black with soot, *Sci. Total Environ.*, *31*, 1–22, 1983.

Nenes, A., S. Ghan, H. Abdul-Razzak, P. Chuang, and J. Seinfeld, Kinetic limitations on cloud droplet formation and impact on cloud albedo, *Tellus B*, *53*, 133–149, 2001.

Nenes, A., W. Conant, and J. Seinfeld, Black carbon radiative effect on cloud microphysics and implications for the aerosol indirect effect: 1. Cloud microphysics, *J. Geophys. Res.*, p. in press, 2002.

Novakov, T., M. Andreae., R. Gabriel, T. Kirchstetter, O. Mayol-Bracero, and V. Ramanathan, Origin of carbonaceous aerosols over the tropical indian ocean: Biomass burning or fossil fuels?, *Geophys. Res. Lett.*, *27*, 4061–4064, 2000.

O'Dowd, C., M. Smith, and S. Jennings, Submicron particle, radon, and soot carbon characteristics over the northeast atlantic, *J. Geophys. Res.*, *98*, 1123–1135, 1993.

O'Dowd, C., J. Lowe, and M. Smith, Coupling sea-salt and sulphate interactions and its impact on cloud droplet concentration predictions, *Geophys. Res. Lett.*, *26*, 1311–1314, 1999.

Podgorny, I., W. Conant, V. Ramanathan, and S. Satheesh, Aerosol modulation of atmospheric and surface solar heating over the tropical Indian Ocean, *Tellus B*, *52*, 947–958, 2000.

Posfai, M., J. Anderson, P. Buseck, and H. Sievering, Soot and sulfate aerosol particles in the remote marine troposphere, *J. Geophys. Res.*, *104*, 21,685–21,693, 1999.

Ramanathan, V., P. Crutzen, J. Lelieveld, A. Mitra, and coauthors, Indian Ocean Experiment: An integrated analysis of the climate forcing and effects of the great Indo-Asian haze, *J. Geophys. Res.*, *106*, 28,369–28,370, 2001.

Seinfeld, J., and S. Pandis, *Atmospheric chemistry and physics: from air pollution to climate change*, John Wiley, New York, 1998.

Tang, I., Thermodynamic and optical properties of mixed-salt aerosols of atmospheric importance, *J. Geophys. Res.*, *102*, 1883–1893, 1997.

Toon, O., and T. Ackerman, Algorithms for the calculation of scattering by stratified spheres, *Appl. Opt*, *20*, 3657–3660, 1981.

Twohy, C., and J. Hudson, Measurements of cloud condensation nucleus spectra within maritime cumulus cloud droplets: Implications for mixing processes, *J. Appl. Meteorol.*, *34*, 815–833, 1995.

Whitby, K., The physical characteristics of sulfur aerosols, *Atmos. Environ.*, *12*, 135–159, 1978.

W. C. Conant, A. Nenes and J. H. Seinfeld, Department of Chemical Engineering, California Institute of Technology, Pasadena CA, 91125. (e-mail: billc@cheme.caltech.edu; nenes@caltech.edu; seinfeld@caltech.edu)

Received February 27, 2002; revised April 5, 2002; accepted April 8, 2002.